Transcranial direct current stimulation alters functional network structure in humans

M. Ruttorf[1*], S. Kristensen[2,3], L.R. Schad[1], J. Almeida[2,3*]

[1] Computer Assisted Clinical Medicine, Medical Faculty Mannheim, Heidelberg University, Germany

[2] Proaction Laboratory, Faculty of Psychology and Educational Sciences, University of Coimbra, Portugal.

[3] Faculty of Psychology and Educational Sciences, University of Coimbra, Portugal.

*Correspondence: michaela.ruttorf@medma.uni-heidelberg.de (M.R.), jorgecbalmeida@gmail.com (J.A.)

Keywords: transcranial direct current stimulation, functional magnetic resonance imaging, network analysis, graph theory, tool network

Abstract

Transcranial direct current stimulation (tDCS) is routinely used in basic and clinical research, but its efficacy has been challenged on a methodological and statistical basis recently. The arguments against tDCS derive from insufficient understanding of how this technique interacts with brain processes physiologically. Because of its potential as a central tool in neuroscience, it is important to clarify whether and how tDCS affects neuronal activity. Here, we investigate influences of offline tDCS on network architecture measured by functional magnetic resonance imaging. Our results reveal a tDCS-induced reorganisation of a functionally-defined network that is dependent on whether we are exciting or inhibiting a node within this network, confirming in a functioning brain, and in a bias free and independent fashion that tDCS influences neuronal activity. Moreover, our results suggest that network-specific connectivity has an important role in defining the effects of tDCS and the relationship between brain states and behaviour.

Introduction

Transcranial direct current stimulation[1,2,3,4,5] (tDCS) has been widely used in the neurosciences[6,7,8,9] for decades. This is so because interfering techniques like tDCS that are assumed to directly modulate neuronal activity are extremely promising for both basic and applied research as they allow for addressing research questions on the causal relationships between brain states and behaviour[10,11,12]. However, the efficacy of tDCS has been put into question recently[13,14,15,16,17] on a methodological and statistical basis. It is thus central to have a closer look at the effects of tDCS on brain activity. Previously, we provided evidence that offline tDCS locally affects neuronal responses in accordance with stimulation polarity (i.e., inhibition or excitation) as measured by functional magnetic resonance imaging (fMRI)[5]. Nevertheless, the global effect of tDCS on functional brain networks in humans is still not well understood[18,19], but is central for a better and more informative understanding

of the mechanisms of tDCS. Based on these previous findings and on the detailed work on living macaques by Krause et al. (2017)[20], here we decided to investigate, in humans, the outcome of tDCS on the underlying functional architecture of the brain as measured by fMRI. There are certain key methodological issues related to the effect of tDCS in the brain that are currently unsolved[21,13,12]. These include understanding the technique's (i) functional focality, i.e. is tDCS limited to local effects on the stimulated area, or do the effects also transfer more globally to the network level as pointed out by Krause et al (2017)[20]; (ii) specificity of stimulation, i.e. is tDCS-induced interference dependent on general processes such as the spatially wide expansion of the electrical field[22], or is it dependent on more neuronally-specified processes such as functional connectivity between regions; or (iii) modulatory effects, i.e. how does tDCS modulate functional connectivity between brain regions. Up to now, there are only two studies evaluating the effect of tDCS on the structure of underlying functional brain networks in depth by means of graph theory: one uses tDCS in combination with resting-state fMRI[23], and the other combines tDCS with electroencephalography[24]. Importantly, none of these examined topology changes in functional brain networks in detail. For this reason and because cognitive functions rely on the processes happening within networks of functionally-connected brain regions rather than on local and isolated areas, we look at how tDCS affects neuronal organisation using a task-based fMRI experiment in combination with offline tDCS. We did so because: (i) task performance enhances neuronal activity resulting in functional connectivity between relevant brain areas being more reliable in terms of graph theory metrics[25]; (ii) tDCS preferentially modulates active neuronal networks, when compared to inactive networks sharing the same anatomical space (activity-selectivity approach)[26]; and (iii) offline tDCS allows us to map the spatio-temporal patterns of functional reorganisation at the systems level[27].

Experimental Layout

We combined tDCS with a task-based paradigm in fMRI using a repeated measures design (see Methods for more details). We asked a group of ten individuals to participate in four experimental sessions, each one separated by at least one week. In the first session, participants went through the fMRI experiment only – as control session – whereas in the second to fourth sessions participants were first subject to tDCS stimulation outside the MR scanner that was immediately followed by the fMRI paradigm. The paradigm consisted on passively watching pictures of tools, animals, faces and places. The tDCS sessions consisted of anodal (typically thought to increase neuronal excitability) or cathodal (typically thought to decrease neuronal excitability)[28,19] stimulation to either the left Inferior Parietal Lobule (IPL) or the right Superior Temporal Sulcus (STS). This resulted in four experimental within-participant groups: anodal stimulation on IPL (AnoIPL), cathodal stimulation on IPL (CatIPL), cathodal stimulation on STS (CatSTS) and control (Ctrl). We chose the left IPL and right STS as target areas because they are highly accessible to the tDCS stimulation technique. Moreover, IPL is known to respond more to images of tools than images of stimuli from other categories[29], whereas STS does not[30]. This is important because by using STS we obtained a tDCS "sham" group to compare tDCS to IPL with – additionally to the control group that serves as ground truth without stimulation. Contrary to classical sham procedures, here participants receive active stimulation to an alternative location to counter doubts which arose recently[31,13] concerning the ability to distinguish classical sham from active stimulation.

We decided to concentrate on brain areas that are dedicated to the processing of tool items (i.e., the tool network[5,32,33]), which left IPL is an exemplary constituent, because effects of tDCS depend on the cognitive/neural processing participants are engaged in – i.e., because this network would be actively processing the tool stimuli presented in our experiment, we could better test the effects of tDCS over this global network. We selected 18 regions of

interest (ROIs) that have been associated with tool processing[29,34,35]. The location of the ROIs can be seen in Figure 1 using BrainNet Viewer software[36] (Version 1.53) as red spheres placed on the ICBM-152 template[37]. The location corresponds to the ROIs' centre coordinates listed in Table 1. Brain networks demonstrate hierarchical modularity (or multi-scale modularity) - i.e. each module contains a set of sub-modules that contains a set of sub-sub-modules, etc[38]. Object recognition – and thereby the tool network as well – is organised in a modular way comparable to colour vision which is shown to be automatic, effortless and informationally encapsulated[39]. Thus, we treated the tool network as a modular network with a subset of highly functional-connected nodes. Keeping this in mind, we are able to test whether tDCS can induce reorganisation over a functional network in the brain, and specifically here over the tool network, beyond the known local effects over the stimulated area[5].

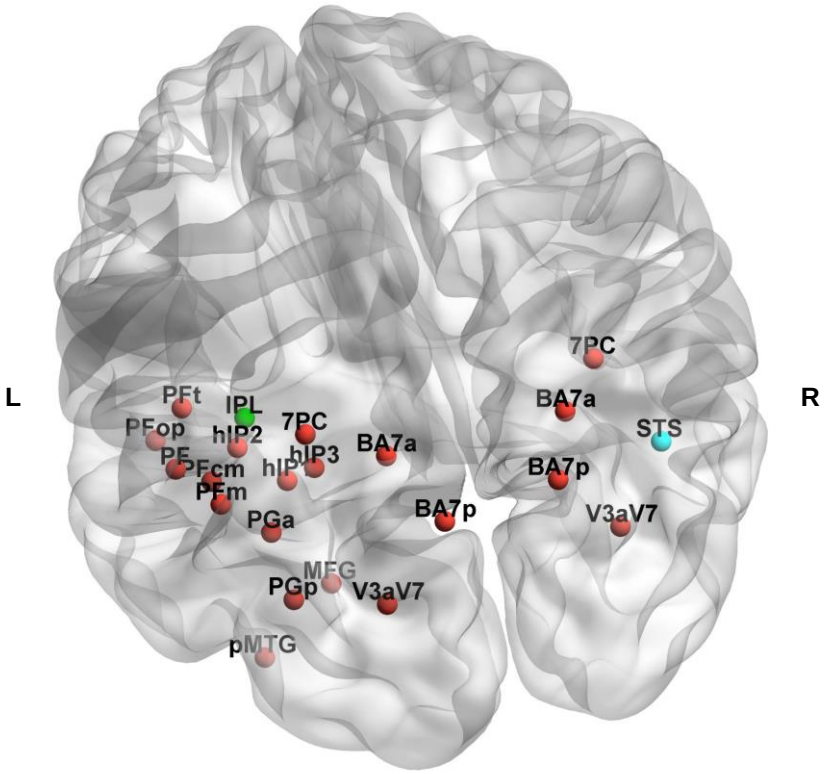

120 **Figure 1: Location of the regions of interest analysed.** Coloured in red are the regions of
121 interest (ROIs) within the tool functional network according to centre coordinates and labels
122 given in Table 1. The location of the stimulation sites is shown either in green (Inferior
123 Parietal Lobule – IPL) or in blue (Superior Temporal Sulcus – STS). L/R denotes the left and
124 right hemisphere, respectively. A video with 360° view of the location of the ROIs is
125 available as Supplementary Information.
126
127 **Graph Theory Analysis**
128 A graph is mathematical description of a network consisting of nodes *N* (here: the ROIs
129 selected) and edges *k* (here: functional "links" between pairs of ROIs). Below, we refer to
130 graphs explicitly because this does not make any assumptions on the nature of the edges but
131 rather emphasises the aspect of mathematical modelling because "network" generally refers to
132 real-world connected systems40. We analysed weighted undirected graphs averaged per group
133 (see Methods for details of graph construction) using Brain Connectivity Toolbox41
134 implemented in MATLAB R2013a (The MathWorks Inc., Natick, MA, USA). Because we
135 were interested in changes in underlying network architecture in the brain between
136 experimental groups we looked at topological graph metrics as community structure and
137 participation coefficients primarily. After graph construction, we checked for *N*,*k*-dependence
138 (see Methods). The number of nodes stays constant (N = 18) in all experimental groups, the
139 number of edges is almost equal between groups (Δk = ±2, k_{max} = 153). Using a repeated
140 measures design, we were only interested in changes between experimental groups. So, we
141 kept the resulting graphs while considering the gain or loss of an edge as an effect of the
142 stimulation (tDCS).
143
144
145

146 **Community Structure**

147 Community structure has been identified as a sensitive marker for organisation in brain
148 networks42. Community structure analysis detects the groups of regions more densely
149 connected between them than expected by chance. The resulting group-level community
150 structure was visualised by assigning a different colour to each community (see Figure 2).
151 This was then displayed by overlaying spheres coloured by community affiliation on the
152 ICBM-152 template as done in Figure 1.

153

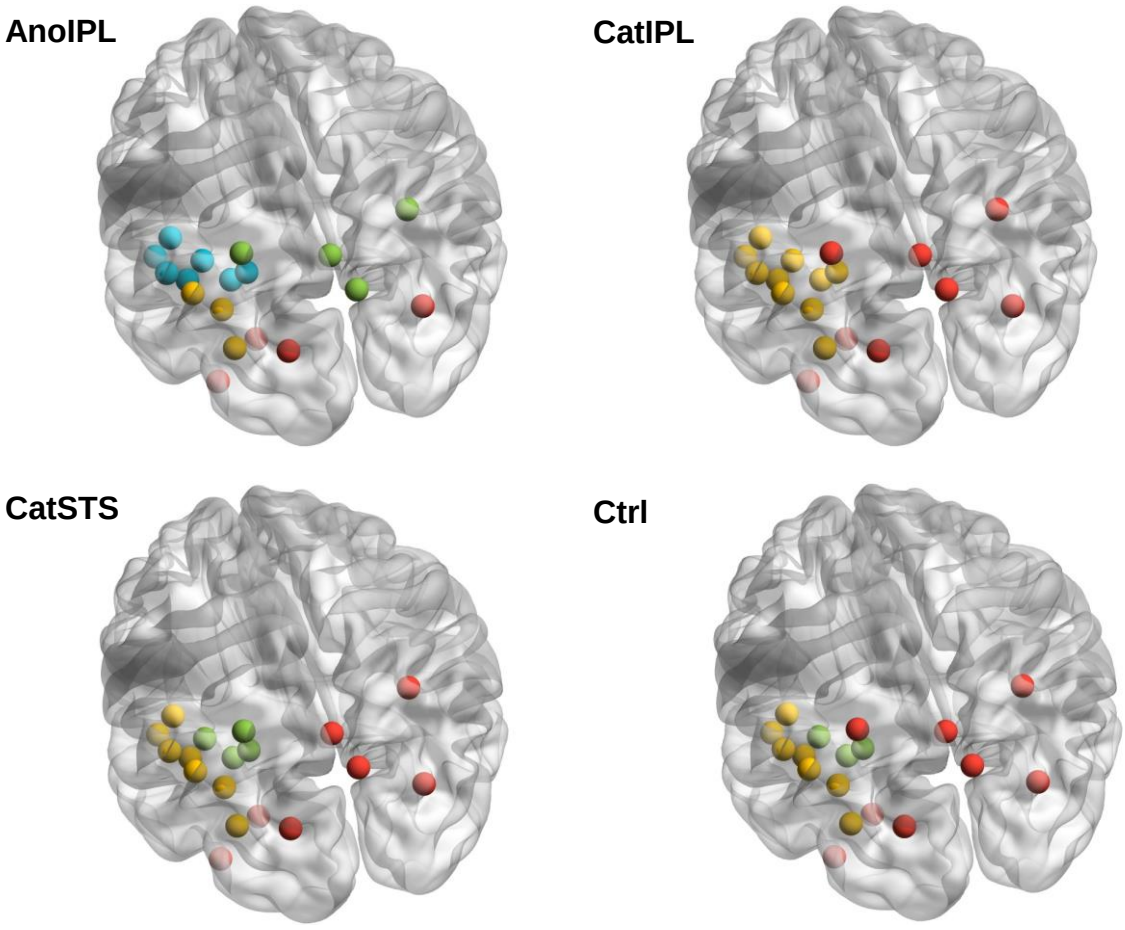

154

155 **Figure 2: Community structure of the tool network.** Within the four experimental groups
156 (AnoIPL, CatIPL, CatSTS and Ctrl), resulting community structures of the tool network are
157 shown. Colours denote different communities; red indicates community I, yellow community
158 II, green community III and blue community IV. Angle of vision kept as in Figure 1. Location
159 of the spheres visualised according to centre coordinates given in Table 1.

The values of modularity Q corresponding to the community structures shown in Figure 2 are almost identical ($\Delta Q = \pm 0.02$). There are three communities in the Ctrl and CatSTS experimental groups, two in CatIPL experimental group and four in AnoIPL experimental group. The communities in Ctrl and CatSTS experimental groups differ minimally from each other. One node changed community assignment (from community III to community I). In AnoIPL experimental group, the community structure intensifies to four whereas in CatIPL experimental group the community structure relaxes to two. We controlled for possible limitations[43] relevant to our experimental layout: the results shown in Figure 2 are neither subject to resolution limit of the objective function[44] nor dependent on the method used to average the correlation coefficients (see Methods for more details). Furthermore, we overlaid the community structure for each experimental group on their averaged weighted temporal correlation matrix before converting to absolute values to verify that negative edge weights are sparser within and denser between communities found[45]. Likewise, we overlaid the community structure for each experimental group on their distance matrix (see Methods) to re-examine that distances within communities are smaller than between communities as shown in Figure 3. We show that the number of communities changed depending on stimulation site and polarity of tDCS. While there is almost no difference in community affiliation when stimulating STS which does not belong to the tool network, there are clear polarity-dependent effects when stimulating IPL.

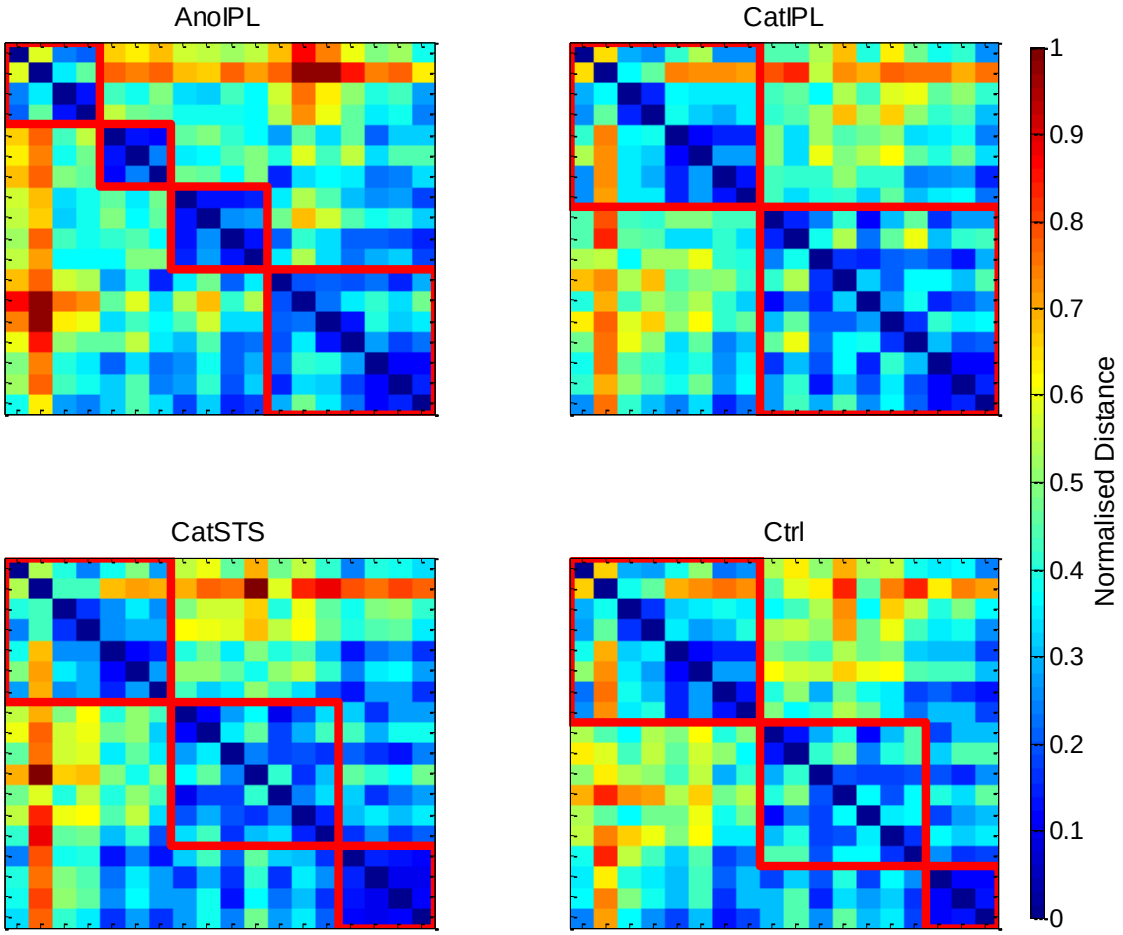

Figure 3: Plots of distance matrices with community structure on top. For the four experimental groups (AnoIPL, CatIPL, CatSTS and Ctrl), normalised distance matrices grouped by communities are shown. The borders of the communities are marked by thick red lines. The colour bar indicates the normalised distance between nodes. The distance is less within communities than between communities throughout experimental groups in all communities found.

Participation Coefficient

While the within-module degree *z* score defines the role of a node in its own community, the participation coefficient *P* is a feature of each node's connectivity relative to the community structure of the entire network46. Nodes with a low value of *P* share connections with other members of the same community, whereas those with a high *P* value serve as connectors

between communities. In Figure 4, the *P* values for the four experimental groups are plotted in the *P*-*z* parameter plane (see Methods for details).

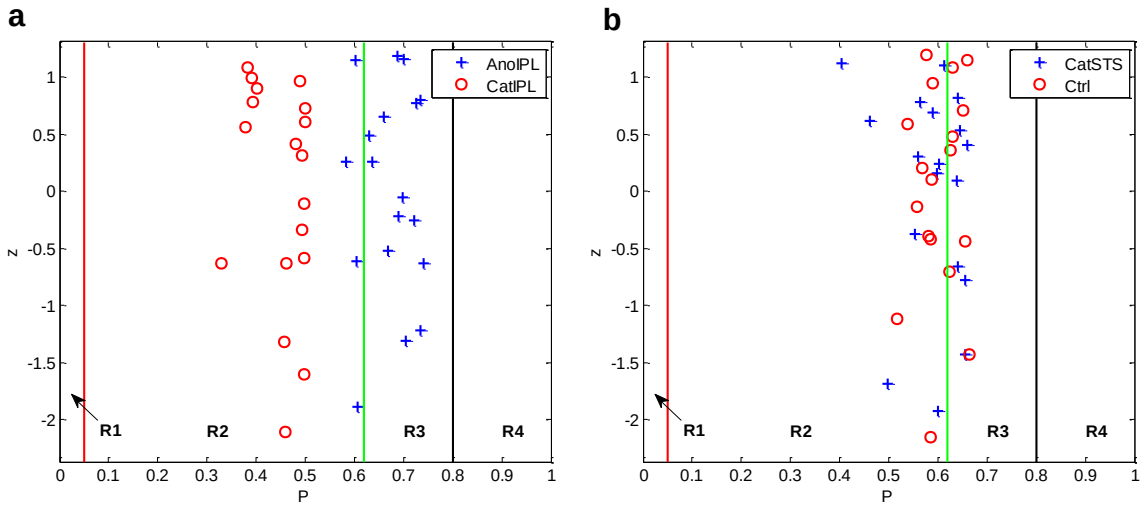

Figure 4: Plots of within-module degree *z* against participation coefficient *P*. For the four experimental groups (AnoIPL, CatIPL, CatSTS and Ctrl), *P*-*z*-plots are shown. The borders of the different regions (R1 – R4, see Methods) are marked by lines. There is a clear difference in distribution between groups AnoIPL and CatIPL (**a**) while there is no difference between groups CatSTS and Ctrl (**b**).

There is a clear difference visible in the distributions of *P* values between CatIPL and AnoIPL experimental groups (Figure 4 (a)) while there seems to be no difference in the other two experimental groups (Figure 4 (b)). Therefore, we analysed the differences in *P* distributions using the Wilcoxon signed-rank test as implemented in MATLAB R2013a. The one-tailed Wilcoxon signed-rank test with $\alpha = 0.01$ shows a significant difference in AnoIPL > CatIPL ($z_{wilcoxon} = 3.70$, $p << 0.01$), AnoIPL > CatSTS ($z_{wilcoxon} = 3.09$, $p << 0.01$), AnoIPL > Ctrl ($z_{wilcoxon} = 2.92$, $p << 0.01$), CatIPL < CatSTS ($z_{wilcoxon} = -3.66$, $p << 0.01$) and CatIPL < Ctrl ($z_{wilcoxon} = -3.70$, $p << 0.01$). There was no significant difference using the two-tailed Wilcoxon signed-rank test with $\alpha = 0.01$ in CatSTS ≠ Ctrl ($z_{wilcoxon} = -0.85$, $p > 0.39$).

Compared to both control experimental groups, more nodes in the AnoIPL experimental group jumped to region R3 while those of the CatIPL experimental group fell back completely to region R2. Finally, we analysed the differences in *z* distributions as well. There was no significant difference using the two-tailed Wilcoxon signed-rank test with $\alpha = 0.01$ between groups: AnoIPL ≠ CatIPL ($z_{wilcoxon} = 0.24$, $p > 0.81$), AnoIPL ≠ CatSTS ($z_{wilcoxon} = 0.20$, $p > 0.84$), AnoIPL ≠ Ctrl ($z_{wilcoxon} = -0.20$, $p > 0.84$), CatIPL ≠ CatSTS ($z_{wilcoxon} = 0.11$, $p > 0.91$), CatIPL ≠ Ctrl ($z_{wilcoxon} = 0.02$, $p > 0.98$) and CatSTS ≠ Ctrl ($z_{wilcoxon} = 0.37$, $p > 0.71$). The role of nodes within their community (*z* value) does not differ significantly in all experimental groups. The role of nodes to other communities (*P* value) changed depending on the kind of stimulation. There was no change compared to Ctrl in the CatSTS experimental group. But in the AnoIPL experimental group, the community structure intensifies and so do the edges between communities. The four modules are more densely connected, the node roles jumped from region R2 (lower *P* values) to region R3 (higher *P* values) having more edges to other communities as compared to both control groups. The opposite is the case in the experimental group CatIPL where the module structure relaxes and so do the node roles. They drop completely to region R2 (lower *P* values) having less edges between communities than in both control experimental groups.

Discussion

Here we show that tDCS to one node of a functional network affects the network architecture as a whole. The results presented here and in Almeida et al. (2017)5 provide a proof of principle that tDCS – delivered through the scalp using currents of 2 mA – can influence neuronal activity in humans. Moreover, they suggests that the effects of tDCS may arise from changed communication patterns (and not just local modulation of signal) that are modified by stimulation polarity and from altered functional connectivity between brain areas.

Crucially, our data shed light to some of the unresolved issues regarding the effects of tDCS at systems level. Namely, that: (i) tDCS is not limited to a local effect on the stimulated area, but exerts polarity-specific effects on the topology of the functional network attached; (ii) this effect is, if anything, only minimally affected by non-specific spread of the tDCS induced electrical field, but is rather dependent on network-specific processing of information; and (iii) at an intermediate scale, tDCS modulates functional connectivity by modular reorganisation.

Our results also show that in anodal tDCS the community structure in a regional and task-related network that is attached to the stimulation site intensifies and this leads to more edges between these communities. The existence of some edges between nodes in different communities acts as topological short-cuts38. This is in line with the results by Polania et al. (2011)23 who came to the conclusion that anodal tDCS increased the functional coupling between left somatomotor cortex (SM1) and neighboured topological regions (left premotor, motor and left parietal cortex) while the number of direct functional connections from left SM1 to topologically distant grey matter voxels decreased significantly. Interestingly, our results contradict Mancini et al.24 who stated that although tDCS is able to change network properties, it does not seem to affect the topological organisation of brain activity at a global level - which is not the case, as we show here.

Our results in the human brain are in line with those of Krause et al. (2017)20 who came to the conclusion that tDCS, in the primate brain, acts by modulating functional connectivity between brain areas. Despite the fact these authors showed – in agreement with Vöröslakos et al. (2018)13 – that in standard tDCS protocols, the electric field reaching the brain is too weak to alter the firing rate of neurons, they also detected a significant increase in anodal stimulation in the local field potential power and coherence in the targeted region when inspecting the effect of tDCS within the same protocols on the brain of living macaques – an

ideal model system because of their thick, dense skull and gyrencephalic cortex similar to humans.

Finally, our data are highly consistent with the proposal that effects of tDCS depend on the level of ongoing activation in the particular functionally-defined target network[47] – when we stimulated a node from another functionally-defined network (i.e., STS) we do not see any tDCS stimulation effects on the tool network.

To conclude, our findings confirm that tDCS influences neuronal activity in humans in a polarity-specific way, and does so in an experimental condition where participants are blind to the polarity of the tDCS stimulation, the measurement (BOLD signal) is bias free in what concerns the status of tDCS – i.e., within a completely independent analysis – and the neural tissue is alive and is engaged in processing incoming stimuli. Moreover, we also show that the flow of information within a functionally-isolated network is altered in a polarity-specific way and that this may be partially the locus of the causal relation between brain states and behaviour.

Methods

Data Acquisition and Pre-processing

We performed a combined tDCS/fMRI experiment on ten healthy adults at a 3T MAGNETOM Trio whole body MR scanner (Siemens Healthineers, Erlangen, Germany). The study adhered to the Declaration of Helsinki and was approved by the Ethic Committee of the Faculty of Medicine, University of Coimbra, Portugal. All participants gave written informed consent after a detailed description of the complete study. Participants went through four experimental sessions: a control session where they participated only in the fMRI experiment; a tDCS anodal session on IPL followed immediately by the fMRI experiment; a tDCS cathodal session on IPL followed immediately by the fMRI experiment; and a tDCS cathodal session on STS followed immediately by the fMRI experiment. All participants went

through the control session first. The order of the tDCS sessions was counterbalanced across participants. Each session was separated by at least a week. During the fMRI experiment, the participants viewed pictures passively in an object processing paradigm (see 5) where we presented images of tools, animals, famous faces, and famous places in a miniblock design48 (each miniblock was restricted to a category). Within each run, miniblocks were pseudo-randomised; all participants completed five runs of this experiment which resulted in recording 455 functional volumes per session.

For analysis of functional brain networks, we extracted the overall mean time series from each of 18 brain regions known to be part of the tool network29,34,35,49,50,51,52 (see Table 1) using a BrainVoyager software (Brain Innovation, Maastricht, The Netherlands) adapted Anatomy Toolbox53. Before extraction of the time series, the functional volumes were pre-processed using BrainVoyager QX 2.8 applying slice-time and 3D motion correction, normalisation to Talairach space54, and z-normalisation. The time series were high-pass filtered (0.008 Hz) to remove low-frequency scanner drift before constructing functional brain networks.

Construction of Functional Brain Networks

Each of the 18 ROIs selected above represents a single node in the resulting functional network. From the overall mean time series, we then obtained a temporal correlation matrix (size 18 x 18) for each participant by computing the Pearson partial correlation coefficients with controlled variables as implemented in MATLAB R2013a between time series of every pair of ROIs, while controlling for effects of noise. As covariates of non-interest for noise correction, we grouped the mean time series from white matter and cerebrospinal fluid extracted for each participant individually along with each participant's motion parameters derived from the realignment step in pre-processing and the effects of the paradigm. The covariate of the paradigm effect was generated by convolving the box–car functions of

paradigm conditions with the standard hemodynamic response function implemented in Statistical Parametric Mapping software (SPM12 (v6685), Wellcome Trust Centre for Neuroimaging, Institute of Neurology, University College London, UK) and was used to remove signal fluctuations of paradigm conditions from the time series. For each temporal correlation calculated, a p-value is given based on Student's t distribution. To minimise the number of false-positives, we used a significance level of $p < 0.002$ (Bonferroni correction) to threshold the temporal correlation matrix of each participant. The remaining correlations can be interpreted as connections or edges between the nodes of the functional network. Here, the values of the correlation coefficients serve as edge weights showing the strength of a relation. While binary values enhance contrast they may also hide important information as edge weights below or above threshold may vary substantially between groups. Weighted graph analysis preserves this information. In our analyses, to avoid negative edge weights we converted them to absolute values because we were interested in any changes between the four experimental groups. It was shown elsewhere[55] that linearly mapping the weight range [-1,1] to [0,1] kept the topology metrics of functional brain networks.

Averaging correlation coefficients

There are at least three different methods to average correlation coefficients: (i) calculation of arithmetic mean of rs which is known to underestimate the true sample mean, (ii) Fisher's z-transform and inverse Fisher's z-transform before and after averaging which is known to overestimate the true sample mean[56] and (iii) Olkin-Pratt estimator[57] which is supposed to be least biased. Because of our sample sizes ($N \leq 10$) which are known to be affected by bias[58] most, we calculated averaged correlation matrices for each group using all three methods. Then, we computed all graph theory metrics listed below with the three group means averaged differently. There were no qualitative differences in the results. The choice of method had no noteworthy influence. For further analysis, we used the Olkin-Pratt estimator

because it is recommended for averaging correlations either across samples or over repeated measures within sample[59].

Graph Theory Metrics

In general, networks (or graphs) are represented as sets of nodes *N* and edges *k*. Graphs are said to be unweighted if edges are either only present or absent – or weighted if edges are assigned weights. Graphs are undirected if edges do not contain directional information and directed if they do. Here, we analysed weighted undirected graphs by means of graph theory using the Brain Connectivity Toolbox[41] (BCT, version 2017-01-15). All graphs analysed are connected graphs. Graph theory metrics depend on the number of *N* and *k*[60] (*N*,*k*-dependence) as well as on the choice of correlation matrix and edge weights[61]. *N*,*k*-dependence can have two effects on graph theory metrics: (i) true effects are masked by opposite effects and (ii) significant effects are introduced. Here, we have primarily looked at graph theory metrics that are less sensitive to changes in *N* and *k* like topological metrics. First, we compared the graphs of the four groups concerning number of edges to address *N*,*k*-dependence of graph metrics. The number of nodes (here: 18) stays constant throughout groups. Then, we looked at topological metrics such as modularity, community structure, within-module degree *z* score, participation coefficient and distance.

Degree: Node degree is the number of links connected to a node. During calculation of node degree using BCT, weight information on edges is discarded[60].

Modularity: The modularity *Q* measures the goodness with which a graph is optimally partitioned into functional subgroups or communities. For weighted graphs, modularity is defined as[62]

$$Q = \frac{1}{2m}\sum_{i,j}\left[A_{ij} - \frac{k_i k_j}{2m}\right]\delta(c_i, c_j)$$

with A_{ij}: weight of edge between i and j, $k_i = \sum_j A_{ij}$: sum of weights of edges attached to vertex i, c_i: community vertex i is assigned to, $\delta(x,y)$ is 1 if $x = y$ and 0 otherwise and $m = 1/2 \sum_{ij} A_{ij}$. Being a scalar value, Q lies in the interval [−1,1], theoretically. If the fraction of within-community edges is no different from what is expected for the randomised network, then Q will be zero. Nonzero values indicate deviations from randomness. Q measures the density of links inside communities compared with links between communities. In this context, the modularity Q is used as an objective function to optimise during graph partitioning: the higher the value of Q the better the partitioning. If the number of edges within communities exceeds the number of edges expected by chance the value of Q is positive.

Community structure: If nodes of a graph can be easily partitioned into sub-units of densely connected nodes, the graph is presumed to have community structure. This implies that communities merely consist of nodes with more densely connections within and more sparsely connections between communities. This definition only holds true for positive edge weights in the first place. Concerning negative edge weights, the assignment of nodes should be done the opposite way compared to positive edge weights, that is negative edges are sparse within and more dense between communities45, a concept evolving from social balance theory63. Although we computed all graph theory metrics using absolute values we cross-checked this limitation by overlaying the community structure for each group on their averaged weighted temporal correlation matrix before converting it to absolute values to verify this issue. As specified before, modularity is an objective function measuring the quality of a graph's community partition. By searching over all possible partitions of a graph, the modularity optimisation method identifies communities that have a high modularity value Q. The detection of a graph's optimal community structure is essential as it may identify

functional sub-units so far unknown that influence the overall behaviour of the graph. The optimal community structure is a partition of the graph into non-overlapping sub-units of nodes maximising the number of edges within sub-units and minimising the number of edges between sub-units64. One limitation of modularity optimisation is the resolution limit44 which could lead to failure in resolving even well-defined small communities. Therefore, it might be possible that communities found are clusters of communities in fact. This might be the case if $k_c < \sqrt{2K}$ where k_c denotes the number of internal edges in the community c and K the total number of edges in the graph. Therefore, it is important to look more closely at the internal structure of all communities found as can be done by using the inequation44

$$\frac{k_c}{K} - \left(\frac{d_c}{2K}\right)^2 > 0$$

with d_c: total degree of nodes in community. If the inequation holds true the community under consideration is actually a single community and not a mixture of two or more smaller ones. All communities found in our analysis comply with the inequation given above. Because community detection using exact modularity optimisation is an NP-hard problem, BCT implemented the Louvain algorithm64 which contains a stochastic element that lets the output vary from run to run. To account for this issue, we ran the algorithm a 1000 times per group and used consensus clustering65 for selection of best community structure for further computations. Once the community structure of a graph is known, the following two graph theory metrics are easily computed.

Within-module degree z score: The internal organisation of a community or module may vary between totally centralised nodes (one or a few nodes connected to all the others) and totally decentralised ones (all nodes having similar number of edges). Nodes are said to fulfil similar roles if they have similar connectivity within a community. The within-module degree *z*-score is a metric of how well-connected a node is to other nodes in a community46 and is defined as

$$z_i = \frac{k_i(c_i) - \bar{k}(c_i)}{\sigma_{k(c_i)}}$$

with c_i: module containing node i, $k_i(c_i)$: within-module degree of i, $k;^{-}(c_i)$: mean of within-module c_i degree distribution and $\sigma_{k(ci)}$: standard deviation of the within-module c_i degree distribution. The higher the values of z, the higher the within-module degrees are and vice versa which implies that nodes with $z \geq 2.5$ can be classified as hub nodes and nodes with $z < 2.5$ as non-hub nodes46. Both types of nodes can be subdivided even further by using the values of the participation coefficient P.

Participation coefficient: The two areas in the z-plane (hub and non-hub nodes) can be fine-grained because of the connections of a node to communities other than its own. Sharing the same z-score, one node might be connected to several nodes in other communities while the other might not. The participation coefficient acts as a measure of diversity of inter-modular connections of nodes46 and is defined as

$$P_i = 1 - \sum_{j=1}^{n_c} \left(\frac{k_{ij}}{k_i}\right)^2$$

with k_{ij}: number of edges of node i to nodes in community j, k_i: total degree of node i and n_c: number of communities detected. The participation coefficient P measures how 'well-distributed' the edges of a node are among different communities. It is close to 1 if the edges are uniformly distributed among all the communities and 0 if the entire edges are within its own community.

Node topology: Based on the idea that nodes with the same role should have similar topological properties, the role of a node can be determined by its location in the P-z-parameter plane which defines how the node is positioned in its own community and relative to others. Guimerà and Amaral46 defined seven regions by dividing the P–z parameter plane

in different areas. Because we are only looking at the tool network, we do not expect to find any hub nodes ($z \geq 2.5$). So, here we only took into account the non-hub nodes area ($z < 2.5$) that was subdivided into four different regions: R1 – nodes with all their edges within their module ($P \leq 0.05$); R2 – nodes with at least 60% of their edges within their module ($0.05 < P \leq 0.62$); R3 – nodes with half of their edges to other modules ($0.62 < P \leq 0.80$); and R4 – nodes with edges homogeneously distributed among all modules ($P > 0.80$). Such nodes were classified as kinless nodes and are said to be mostly found in network growth models, but not in real-world networks.

Distance: The distance matrix shows the length of shortest paths between all pairs of nodes. Each entry stands for the number of edges that have to be traversed to get from one node to another. By using a weighted correlation matrix, higher correlation coefficients denote shorter distances. We converted the weighted correlation matrices to length by inversion of weights and fed them into Dijkstra algorithm66 to compute the distance between nodes.

References

1. Yavari, F. *et al*. Basic and functional effects of transcranial Electrical Stimulation (tES) – An introduction. *Neurosci Biobehav Rev* **85**, 81 – 92 (2018).
2. Das, S., Holland, P., Frens, M.A. & Donchin, O. Impact of Transcranial Direct Current Stimulation (tDCS) on Neuronal Functions. *Front Neurosci* **10**, Article 550 (2016).
3. Giordano *et al.* Mechanisms and Effects of Transcranial Direct Current Stimulation. *Dose-Response* **15**, 1 – 22 (2017).
4. Woods, A.J. *et al.* A technical guide to tDCS, and related non-invasive brain stimulation tools. *Clin Neurophysiol* **127**, 1031 – 1048 (2016).

5. Almeida, J. *et al.* Polarity-specific transcranial Direct Current Stimulation effects on object-selective neural responses in the Inferior Parietal Lobe. *Cortex* **94**, 176 - 181 (2017).
6. Brunoni, A.R., Fregni, F. & Pagano, R.L. Translational research in transcranial direct current stimulation (tDCS): a systematic review of studies in animals. *Rev Neurosci* **22**, 471 – 481 (2011).
7. Cappon, D., Jahanshahi, M. & Bisiacchi, P. Value and Efficacy of Transcranial Direct Current Stimulation in the Cognitive Rehabilitation: A Critical Review Since 2000. *Front Neurosci* **10**, Article 157 (2016).
8. Dedoncker, J., Brunoni, A.R., Baeken, C. & Vanderhasselt, M. A Systematic Review and Meta-Analysis of the Effects of Transcranial Direct Current Stimulation (tDCS) Over the Dorsolateral Prefrontal Cortex in Healthy and Neuropsychiatric Samples: Influence of Stimulation Parameters. *Brain Stimul* **9**, 501 – 517 (2016).
9. Monti, A. *et al.* Transcranial direct current stimulation (tDCS) and language. *J Neurol Neurosurg Psychiatry* **84**, 832 – 842 (2013).
10. Parkin, B. L., Ekhtiari, H. & Walsh, V. F. Non-invasive Human Brain Stimulation in Cognitive Neuroscience: A Primer. *Neuron* **87**, 932 – 945 (2015).
11. de Graaf, T. A. & Sack, A. T. Using brain stimulation to disentangle neural correlates of conscious vision. *Front. Psychol* **5**, 1 – 13 (2014).
12. Saiote, C., Turi, Z., Paulus, W. & Antal, A. Combining functional magnetic resonance imaging with transcranial electrical stimulation. *Front Hum Neurosci* **7**, Article 435 (2013).
13. Vöröslakos, M. *et al.* Direct effects of transcranial electric stimulation on brain circuits in rats and humans. *Nat Commun* **9**, 483 (2018).

14. Horvath, J.C., Carter, O. & Forte, J.D. Transcranial direct current stimulation: five important issues we aren't discussing (but probably should be). *Front Syst Neurosci* **8**, Article 2 (2014).

15. Horvath, J.C., Forte, J.D. & Carter, O. Evidence that transcranial direct current stimulation (tDCS) generates little-to-no reliable neurophysiologic effect beyond MEP amplitude modulation in healthy human subjects: A systematic review. *Neuropsychologia* **66**, 213 – 236 (2015).

16. Horvath, J.C., Carter, O. & Forte, J.D. No significant effect of transcranial direct current stimulation (tDCS) found on simple motor reaction time comparing 15 different simulation protocols. *Neuropsychologia* **91**, 544 – 552 (2016).

17. Mancuso, L.E., Ilieva, I.P., Hamilton, R.H. & Farah, M.J. Does transcranial direct current stimulation improve healthy working memory?: A meta-analytic review. *J Cogn Neurosci* **28**, 1063–1089 (2016).

18. Luft, C.D., Pereda, E., Banissy, M.J. & Bhattacharya, J. Best of both worlds: promise of combining brain stimulation and brain connectome. *Front Syst Neurosci.* **8**, Article 32 (2014).

19. Stagg, C. J. & Nitsche, M. A. Physiological Basis of Transcranial Direct Current Stimulation. *Neuroscientist* **17**, 37 – 53 (2011).

20. Krause, M.R. *et al.* Transcranial Direct Current Stimulation Facilitates Associative Learning and Alters Functional Connectivity in the Primate Brain. *Curr Biol* **27**, 3086 – 3096 (2017).

21. Filmer, H.L., Dux, P.E. & Mattingley, J.B. Applications of transcranial direct current stimulation for understanding brain function. *Trends Neurosci* **37**, 12 (2014).

22. Bikson, M., Rahman, A. & Datta, A. Computational Models of Transcranial Direct Current Stimulation. *Clin EEG Neurosci* **43**, 176 – 183 (2012).

512 23. Polanía, R., Paulus, W., Antal, A. & Nitsche, M.A. Introducing graph theory to track
513 for neuroplastic alterations in the resting human brain: a transcranial direct current
514 stimulation study. *NeuroImage* **54**, 2287 – 2296 (2011).
515 24. Mancini, M. *et al.* Assessing cortical synchronization during transcranial direct current
516 stimulation: A graph-theoretical analysis. *NeuroImage* **140**, 57 – 65 (2016).
517 25. Wang, J. *et al.* Test–Retest Reliability of Functional Connectivity Networks During
518 Naturalistic fMRI Paradigms. *Hum Brain Mapp* **38**, 2226 – 2241 (2017).
519 26. Bikson, M. & Rahman, A. Origins of specificity during tDCS: anatomical, activity-
520 selective, and input-bias mechanisms. *Front Hum Neurosci* **7**, Article 688, (2013).
521 27. Venkatakrishnan, A. & Sandrini, M. Combining transcranial direct current stimulation
522 and neuroimaging: novel insights in understanding neuroplasticity. *J Neurophysiol*
523 **107**, 1 – 4 (2012).
524 28. Senço, N.M. et al. Transcranial direct current stimulation in obsessive-compulsive
525 disorder: emerging clinical evidence and considerations for optimal montage of
526 electrodes. *Expert Rev Med Devic* **12**, 381 – 391 (2015).
527 29. Almeida, J., Fintzi, A. & Mahon, B. Tool manipulation knowledge is retrieved by way
528 of the ventral visual object processing pathway. *Cortex* **49**, 2334 – 2344 (2013).
529 30. Hein, G. & Knight, R.T. Superior Temporal Sulcus—It's My Area: Or Is It? *J Cogn*
530 *Neurosci* **20**, 2125 – 2136 (2008).
531 31. O'Connell *et al*. Rethinking Clinical Trials of Transcranial Direct Current Stimulation:
532 Participant and Assessor Blinding Is Inadequate at Intensities of 2mA. *PLoS ONE* **7**,
533 e47514 (2012).
534 32. Johnson-Frey, S.H., Newman-Norlund, R. & Grafton, S.T. A Distributed Left
535 Hemisphere Network Active During Planning of Everyday Tool Use Skills. *Cereb*
536 *Cortex* **15**, 681 – 695 (2005).

537 33. Chen, Q., Garcea, F.E., Almeida, J. & Mahon, B.Z. Connectivity-based constraints on
538 category-specificity in the ventral object processing pathway. *Neuropsychologia* **105**,
539 184 - 196 (2017).
540 34. Kristensen, S., Garcea, F.E., Mahon, B.Z. & Almeida, J. Temporal frequency tuning
541 reveals interactions between the dorsal and ventral visual streams. *J Cogn Neurosci*
542 **28**, 1295 – 1302 (2016).
543 35. Chao, L.L., Haxby, V.J. & Martin, A. Attribute-based neural substrates in temporal
544 cortex for perceiving and knowing about objects. *Nat Neurosci* **2**, 913 – 919 (1999).
545 36. Xia, M., Wang, J. & He, Y. BrainNet Viewer: A Network Visualization Tool for
546 Human Brain Connectomics. *PLoS ONE* **8**, e68910 (2013).
547 37. Mazziotta, J. *et al.* A probabilistic atlas and reference system for the human brain:
548 International Consortium for Brain Mapping (ICBM). *Phil Trans R Soc B* **356**, 1293 –
549 1322 (2001).
550 38. Meunier, D., Lambiotte, R. & Bullmore, E.T. Modular and hierarchically modular
551 organization of brain networks. *Front Neurosci* **4**, Article 200 (2010).
552 39. Zeki, S. & Bartels, A. The autonomy of the visual systems and the modularity of
553 conscious vision. *Phil Trans R Soc B* **353**, 1911 – 1914 (1998).
554 40. De Vico Fallani, F., Richiardi, J., Chavez, M. & Achard, S. Graph analysis of
555 functional brain networks: practical issues in translational neuroscience. *Phil Trans R*
556 *Soc B* **369**, 20130521 (2014).
557 41. Rubinov, M. & Sporns, O. Complex network measures of brain connectivity: Uses and
558 interpretations. *NeuroImage* **52**, 1059 – 1069 (2010).
559 42. He, Y. *et al*. Uncovering Intrinsic Modular Organization of Spontaneous Brain
560 Activity in Humans. *PLoS ONE* **4**, e5226 (2009).
561 43. Sporns, O. & Betzel, R.F. Modular Brain Networks. *Annu Rev Psychol* **67**, 613 – 640
562 (2016).

563 44. Fortunato, S. & Barthélemy, M. Resolution limit in community detection. *Proc Nat*
564 *Acad Sci USA* **104**, 36 – 41 (2007).
565 45. Traag, V.A. & Bruggeman, J. Community detection in networks with positive and
566 negative links. *Phys Rev E* **80**, 036115 (2009).
567 46. Guimerà, R. & Nunes Amaral, L.A. Functional cartography of complex metabolic
568 networks. *Nature* **433**, 895 – 900 (2005).
569 47. Fertonani, A. & Miniussi, C. Transcranial Electrical Stimulation: What We Know and
570 Do Not Know About Mechanisms. *Neuroscientist* **23**, 109 – 123 (2017).
571 48. Fintzi, A.R. & Mahon, B.Z. A Bimodal Tuning Curve for Spatial Frequency Across
572 Left and Right Human Orbital Frontal Cortex During Object Recognition. *Cereb*
573 *Cortex* **24**, 1311 – 1318 (2014).
574 49. Macdonald, S.N. & Culham, J.C. Do human brain areas involved in visuomotor
575 actions show a preference for real tools over visually similar non-tools?
576 *Neuropsychologia* **77**, 35 – 41 (2015).
577 50. Vingerhoets, G., Acke, F., Vandemaele, P. & Achten, E. Tool responsive regions in
578 the posterior parietal cortex: Effect of differences in motor goal and target object
579 during imagined transitive movements. *NeuroImage* **47**, 1832 – 1843 (2009).
580 51. Peeters, R.R., Rizzolatti, G. & Orban, G.A. Functional properties of the left parietal
581 tool use region. *NeuroImage* **78**, 83 – 93 (2013).
582 52. Creem-Regehr, S.H. & Lee, J.N. Neural representations of graspable objects: are tools
583 special? *Cognitive Brain Res* **22**, 457 – 469 (2005).
584 53. Eickhoff, S. *et al.* A new SPM toolbox for combining probabilistic cytoarchitectonic
585 maps and functional imaging data. *NeuroImage* **25**, 1325 – 1335 (2005).
586 54. Talairach, P. & Tournoux, J. *Co-Planar Stereotaxic Atlas of the Human Brain*
587 (Thieme, 1988).

588 55. Rubinov, M. & Sporns, O. Weight-conserving characterization of complex functional
589 brain networks. *NeuroImage* **56**, 2068 – 2079 (2011).
590 56. Corey, D.M, Dunlap, W.P. & Burke, M.J. Averaging Correlations: Expected Values
591 and Bias in Combined Pearson's rs and Fisher's z Transformation. *J Gen Psychol* **125**,
592 245 – 261 (1998).
593 57. Olkin, I. & Pratt, J. W. Unbiased estimation of certain correlation coefficients. *Ann*
594 *Math Stat* **29**, 201 – 211 (1958).
595 58. Zimmerman, D.W., Zumbo, B.D. & Williams, R.H. Bias in Estimation and
596 Hypothesis Testing of Correlation. *Psicológica* **24**, 133 – 158 (2003).
597 59. Alexander, R.A. A note on averaging correlations. *B Psychonomic Soc* **28**, 335 – 336
598 (1990).
599 60. van Wijk, B.C.M., Stam, C.J. & Daffertshofer, A. Comparing Brain Networks of
600 Different Size and Connectivity Density Using Graph Theory. *PLoS ONE* **5**, e13701
601 (2010).
602 61. Phillips, D.J. *et al*. Graph theoretic analysis of structural connectivity across the
603 spectrum of Alzheimer's disease: The importance of graph creation methods.
604 *NeuroImage: Clinical* **7**, 377 – 390 (2015).
605 62. Newman, M.E.J. Analysis of weighted networks. *Phys Rev E* **70**, 056131 (2004).
606 63. Harary, F. On the notion of balance of a signed graph. *Mich Math J* **2**, 143 – 146
607 (1953).
608 64. Blondel, V.D, Guillaume, J.-L., Lambiotte, R. & Lefebvre, E. Fast unfolding of
609 communities in large networks. *J Stat Mech-Theory E* **2008**, P10008 (2008).
610 65. Lancichinetti, A. & Fortunato, S. Consensus clustering in complex networks. *Sci Rep*
611 **2**, 336 (2012).
612 66. Dijkstra, E.W. A Note on Two Problems in Connexion with Graphs. *Numer Math* **1**,
613 269 – 271 (1959).

Acknowledgements

This research was supported by a Foundation for Science and Technology of Portugal and Programa COMPETE grant (PTDC/ MHC-PCN/0522/2014) to J.A. M.R. and J.A. were supported by Deutscher Akademischer Austauschdienst (Projekt-ID 57212180) and CRUP. S.K. is supported by a Foundation for Science and Technology of Portugal and Programa COMPETE grant (PTDC/MHC-PCN/0522/2014). This research was supported by German Research Foundation grant SCHA 546/22-1 to L.R.S.

Author contributions

M.R. performed data analyses, prepared the graphics and wrote the paper. S.K. performed data analysis. L.R.S. contributed ideas. J.A. conceived and designed the project, and critically revised the manuscript. M.R. and J.A. interpreted the data.

626 **Table 1. Overview of brain regions in analysed functional network**

Lobe	Hemisphere	Structure	Brodman area [BA]	Label	Talairach Coordinates		
					X	Y	Z
ROIs of Tool Network							
temporal	left	posterior middle temporal gyrus	BA 37	pMTG	-42	-62	-7
temporal	left	middle fusiform gyrus	BA 37	MFG	-24	-48	-8
occipital	left	extrastriate visual cortex	BA 19	V3aV7	-23	-80	24
occipital	right	extrastriate visual cortex	BA 19	V3aV7	25	-78	27
parietal	left	anterior angular gyrus	BA 39	PGa	-41	-63	33
occipital	left	posterior angular gyrus	BA 39	PGp	-40	-73	24
parietal	left	superior parietal lobe (anterior parts)	BA 7	BA7a	-18	-64	49
	right				18	-65	50
parietal	left	superior parietal lobe (posterior parts)	BA 7	BA7p	-10	-76	40
	right				13	-76	44
parietal	left	lateral superior parietal lobe	BA 7	7PC	-31	-55	50
parietal	right	lateral superior parietal lobe	BA 7	7PC	27	-54	49
parietal	left	supramarginal gyrus	BA 40	PF	-53	-41	31
temporal	left	supramarginal gyrus	BA 40	PFcm	-45	-39	21
parietal	left	supramarginal gyrus	BA 40	PFm	-48	-54	34
parietal	left	supramarginal gyrus	BA 40	PFop	-53	-28	24
parietal	left	supramarginal gyrus	BA 40	PFt	-48	-29	33
parietal	left	intraparietal sulcus	BA 7/40	hIP1	-34	-52	34
parietal	left	intraparietal sulcus	BA 7/40	hIP2	-42	-44	37
parietal	left	superior parietal lobe	BA 7/40	hIP3	-29	-54	38
Stimulation Sites							
parietal	left	inferior parietal lobe	BA 40	IPL	-38	-37	36
temporal	right	superior temporal sulcus	BA 37	STS	44	-45	6

627 Here, we list the names of the brain areas, labels used in the text and centre coordinates (x,y,z)
628 in Talairach space of the regions of interests (ROI) of the tool network and the stimulation
629 sites. The anterior and posterior parts of the superior parietal lobe are bilateral ROIs.